

# Comparison of Convergence-Zone-Measured Sound Pressures in the Deep Ocean with Pressures Computed from the Sound Speed-Depth Function

R. L. STEINBERGER

*Propagation Branch  
Sound Division*

August 5, 1965



**PLEASE RETURN THIS COPY TO:**

NAVAL RESEARCH LABORATORY  
WASHINGTON, D.C. 20390  
ATTN: CODE 2028

Because of our limited supply you are requested to return this copy as soon as it has served your purposes so that it may be made available to others for reference use. Your cooperation will be appreciated.

NDW-NRL - 5070/2035 (10-67)

**U.S. NAVAL RESEARCH LABORATORY**  
Washington, D.C.

1917

1917

1917

1917

1917



## ABSTRACT

This report is a sequel to an earlier report (NRL Report 6123) in which the sound speed  $c$  was determined as a function of the depth  $z$  in deep-ocean waters north of Puerto Rico. Computational methods were also developed and used to obtain numerical values for the horizontal range between the sound source and the zone where the emitted acoustic waves converge to give signal (pressure) enhancement. The present report is concerned with computing the detailed distribution of sound pressure, by means of ray diagrams and field measurements, in the zone. On the basis of simple wave theory, convergence zone ranges and pressure values are derived from the  $c(z)$  function for three basic ray fans which overlap at the zone. It is found that both the horizontal range determinations (from 64.34 to about 70 km) and the acoustic pressure values within the zone agree favorably with measured values. By utilizing deep-ocean measurements, the resultant acoustic pressures were free of confusion from bottom scattering and the complexity of many refraction paths.

## PROBLEM STATUS

This is an interim report on the problem; work is continuing.

## AUTHORIZATION

NRL Problem S01-01  
Project RF 101-03-45-5250

Manuscript submitted March 8, 1965.

CONFIDENTIAL

COMPARISON OF CONVERGENCE-ZONE-MEASURED  
SOUND PRESSURES IN THE DEEP OCEAN WITH PRESSURES  
COMPUTED FROM THE SOUND SPEED-DEPTH FUNCTION

## INTRODUCTION

The convergence of rays in a refractive medium is a physical phenomenon in many wave transmitting situations. The special convergence case discussed here takes place in what will be called simply the "zone." It occurs when acoustic rays are projected downward, close to the horizontal, into the deep ocean and the refraction is such as to turn each ray upward after reaching a "vertex" depth, returning then at a horizontal range of about 65 km to the depth level of the source where the acoustic signal is measured. The pressure signal measured is the sum of the acoustic pressures at the point of measurement. The sound pressure distribution in the zone will be constructed on the basis of the refraction situation existing in the deep Atlantic ocean on October 26, 1960, at latitude 19°19'N, longitude 66°12.5'W. Refraction and geographic conditions are described in NRL Report 6123 (1).

## RAY GEOMETRY

Assuming circular symmetry about the source, the acoustic rays are plane curves (see Fig. 2a of Ref. 1) in the  $xz$  vertical plane through the source. The difficult three-dimensional geometry of bundles of rays, which are general space curves, may then be set aside in favor of the simple plane geometry of plane ray fans in the vertical two-dimensional ocean cross section.

In order to delineate the geometry of convergence and make an estimate of enhancement of signal in the zone, it is necessary that a number of rays (Table 1) constituting the principal convergence fan be drawn with emission angles  $\theta_0$  starting at 90 degrees and ranging downward to about 75 degrees. The vertex  $Z$  for the 75-degree ray is at a depth of 8036 m. The ocean bottom is at 7498 m. The 75-degree ray thus strikes the bottom at an angle of  $\theta = \sin^{-1} [p/\eta(z)] = 83.85$  degrees, measured from the plumb line. The function  $\eta(z)$  is equal to  $1/c(z)$  where  $c(z)$ , the speed of sound, is a function of depth  $z$  (see Ref. 1). For the present, attention is confined to the lower half-space bounded on top by the source plane. Concentration of the convergence rays at the zone gives rise to signal enhancement over single-ray inverse-square-distance spreading of energy. The rays in the fan strike the circular zone at varying radial distances (ranges), depending upon the value of  $\theta_0$ . Under idealized conditions there is a sharp, short-range edge to the zone marked by the one ray of minimum range accumulation. This is discussed in Ref. 2 for the case of a simple, mathematically defined  $c(z)$  function. The range  $2X$  to the zone edge is determined in the present case by numerical reduction of the empirical data associated with a fan wherein the minimum ray turns out to have an emission angle of 87.1 degrees (Fig. 1). Nine rays ranging from  $\theta_0 = 90$  degrees to  $\theta_0 = 75$  degrees were used in the construction of Fig. 1, although the complete range of emission angles is 90 degrees. Each computation leads to the specification of a segment of the particular ray function  $x(z)$  starting at the source point  $x_0, z_0$ , Fig. 2, and ending at its vertex point  $X, Z$ . In this range of values for  $z$  the ray functions  $x(z)$  are single valued in  $z$ . Beyond the vertex  $X, Z$  the ray, defined by a new  $x(z)$ , turns upward toward the zone at the source level along a path which is the image, in the line  $x = X$ , of the  $x_0, z_0$  to  $X, Z$  segment of the ray. The horizontal distance from the source to the zone is  $2X$ .

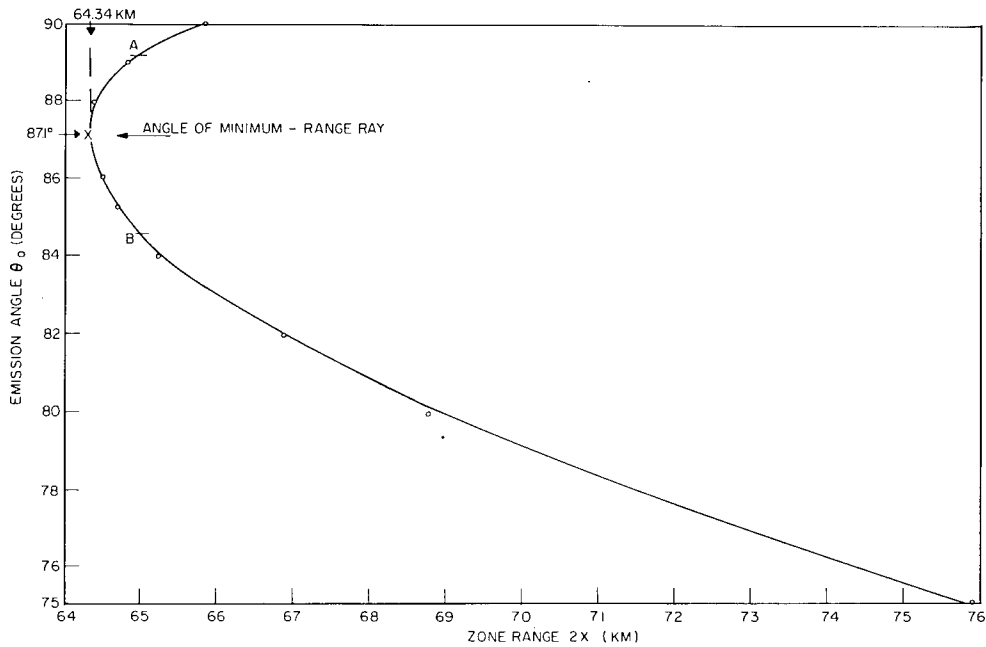


Fig. 1 - Acoustic ray emission angle  $\theta_0$  vs zone range  $2X$  for nine select rays. The emission angle for a given ray is measured from the vertical (plumb) line to the ocean surface. For the rays emitted at a given angle and in a circular pattern about the source, the zone range is defined as the distance between the acoustic source and a circle, surrounding the source, to which the rays are refracted up to the ocean level of the source. For a fan of acoustic rays emitted at various angles, the one ray that travels (during refraction) a minimum distance from the source back up to the source depth defines the edge of the convergence zone. The curve shown allows a representative of the zone range  $2X$  as a function of  $\theta_0$ .

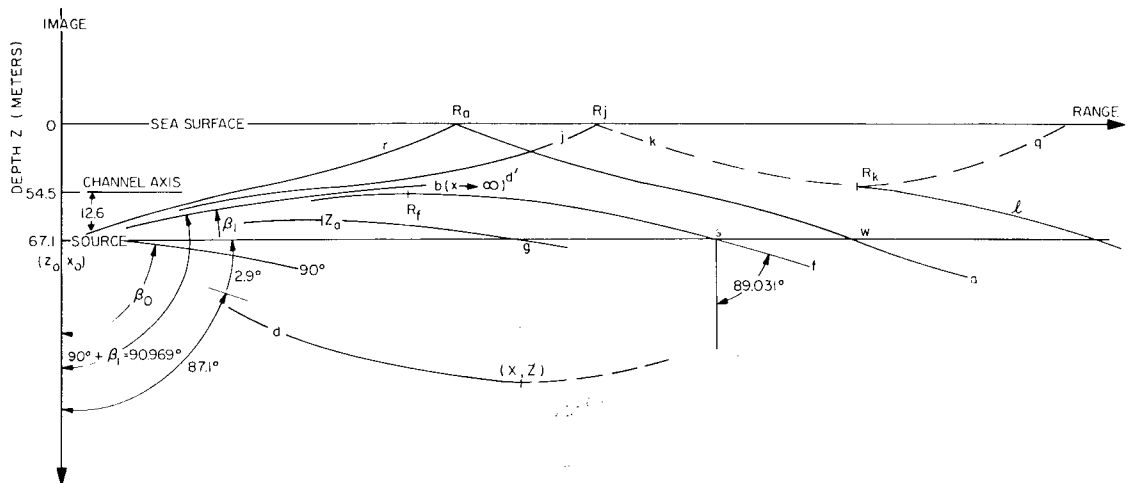


Fig. 2 - Depth  $z$  vs range  $x$  for typical acoustic rays refracted and reflected in the ocean. The rays originate at the point  $x_0, z_0$  and are initially emitted at the angles indicated.

RAY EMISSION ANGLE AND RANGES

The stratified nature of the refraction functions  $T(z)$  of temperature and  $S(z)$  of salinity, as observed in the deep ocean and the 900-ft scale of the bathythermograph, suggested a computational subdivision of the ocean below the source into three layers (Table 1). The line made by joining end-to-end the segments of the particular ray in the three layers is the source-to-vertex ray segment. Invoking symmetry about  $x = X$ , the whole convergence ray becomes the sum of this source-to-vertex segment and its image. The numerical values for the several range accumulations are gathered together in Table 1 under the separate emission angle headings and ocean layers I, II, III. The symbol  $X$  is used for the accumulation of range from source to vertex.

The entries under  $2X$  in Table 1 form the important relationship between zone range and emission angle  $\theta_o$ . This function  $2X(\theta_o)$  for the principal convergence fan, as read from the nine rays of Table 1, is plotted in Fig. 1. In the principal convergence fan the rays pass from source to zone without surface reflection or refractive bending above the source. They are confined to the half-space below the source.

Table 1  
Horizontal Zone Ranges for Nine Typical Rays  
in the Principal Convergence Fan of Rays

Ocean Layer*	Range (km) for Ocean Layer and Emission Angle Indicated		
	$\theta_o = 90^\circ$	$\theta_o = 88.95^\circ$	$\theta_o = 88^\circ$
I	2.93	2.45	2.13
II	7.00	6.97	6.91
III	23.00	23.02	23.18
$X^\dagger$	32.93	32.42	32.33
$2X(\theta_o)^\ddagger$	65.85	64.83	64.43
	$\theta_o = 86^\circ$	$\theta_o = 85.3^\circ$	$\theta_o = 84^\circ$
I	1.70	1.58	1.40
II	6.70	6.57	6.38
III	23.84	24.22	24.86
$X$	32.24	32.37	32.63
$2X(\theta_o)$	64.48	64.74	65.27
	$\theta_o = 82^\circ$	$\theta_o = 80^\circ$	$\theta_o = 75^\circ$
I	1.18	1.00	0.72
II	6.01	5.60	4.62
III	26.27	27.80	32.61
$X$	33.45	34.40	37.95
$2X(\theta_o)$	66.91	68.79	75.89

\*Layer I extends from 67.1 to 280 m depth; II extends from 280 to 2000 m depth; and III extends from 2000 to  $Z$  m depth.

$\dagger X$  = accumulated horizontal range from acoustic source to ray vertex.

$\ddagger 2X(\theta_o)$  = horizontal range from acoustic source to ray fan convergence zone edge.

At an angle of  $\theta_o = 87.1$  degrees the range to the zone has the least value of  $2 \times 32.17$  (= 64.34) km. At other  $\theta_o$  angles, greater or less than 87.1 degrees, the rays reach the zone at greater ranges. The principal fan of rays between 0 and 90 degrees contains no rays of zone range less than 64.34 km. This is the short-range limit of the zone. In the half-space below the source level near the zone, ranges shorter than the limit are in the "shadow," whose lower border is formed by the 90-degree ray. The shadow is not perfect if the source is below the surface because rays from the water above the source may penetrate to the hydrophone. The rays responsible for this will be discussed later. At a range in the zone (say 65 km) beyond the limit, two rays (e.g., A and B in Fig. 1) in the principal fan pass through each point, say P, at 65 km in the zone.

### RANGE ACCUMULATION

The coordinates of the 90-degree ray, Fig. 2, are important because this ray is the upper boundary of the principal convergence fan. The 90-degree ray is exceptional in that the source point is also a vertex (an upper vertex — see Fig. 2b, Ref. 1), and errors of large magnitude can enter the integrand  $D^{-1/2}$ \* in the integral  $x = p \int D^{-1/2} dz$  when integration is attempted. To avoid the difficulty, Eq. (1) below may be used over the short depth interval  $0 < h < 12.9$  m near the source, thus bridging across the uncertain  $D^{-1/2}$  range between the depths  $z = 67.1$  m and  $z = 80$  m. The range accumulation between the points  $x_1$  and  $x_2$  is then

$$x_2 - x_1 = p \sqrt{2/v} \int (2D_n/v + 2mh/v + h^2)^{-1/2} dh. \dagger \quad (1)$$

The source is at an upper vertex where  $D_n = 0$  and the integration can be accomplished by using Form 181, page 300, or Form 216, page 302, in Ref. 3. When the lower limits  $h = 0$  and  $x_1 = 0$  are inserted, the ray accumulation  $x_2$  becomes

$$x_2 = p \sqrt{2/v} \ln \left[ (v/m) (\sqrt{h^2 + 2mh/v} + h + m/v) \right]. \quad (2)$$

The pertinent constants and parameters for this situation are

$$p = 6.4733 \times 10^{-4}$$

$$v = 17.8 \times 10^{-13}$$

$$m = 19.0 \times 10^{-12}$$

$$m/v = 10.68$$

$$v/m = 0.0936$$

$$h = 12.9$$

$$\sqrt{2/v} = 1.06 \times 10^6.$$

When these numbers are inserted into Eq. (2), the value of  $x_2$  becomes 984 m. This is the range accumulation for the ray of emission angle  $\theta_o = 90$  degrees when travelling from the source at a depth of  $z_1 = 67.1$  m to the depth  $z = 80$  m. The 90-degree ray

\* $D = \eta^2 - p^2$  (1).

† Ref. 1, Eq. (19) with  $\sqrt{2/v}$  factored out.

bends downward, in consonance with the fact that  $z$ , measured downward, is positive. The depth increment  $h$  is also positive and, when inserted into the equation, gives a real value of  $x_2$ .

The whole range accumulation  $x_2 - x_1$  for the 90-degree ray in Layer I is given by

$$\frac{(x_2 - x_1)}{P} = \int_{67.1}^{280} D^{-1/2} dz = \int_{67.1}^{80} + \int_{75}^{285} - \int_{75}^{80} - \int_{280}^{285}$$

where the integrand is omitted for brevity. The right-hand equality gives

$$\int_{67.1}^{280} = \frac{984.0}{P} + 10 \sum_{80}^{280} D^{-1/2} - 5 \left\langle D^{-1/2} \right\rangle_{75}^{80} - 5 \left\langle D^{-1/2} \right\rangle_{280}^{285}$$

So,

$$\begin{aligned} x_2 - x_1 &= 984.0 + 10p \times 3.37 \times 10^{+3} - 5p[67 \times 10^{+3} + 9.6 \times 10^{+3}] \\ &= 984.0 + p \times 3014 \times 10^{+3} \\ &= 984 + 1950 = 2934 . \end{aligned}$$

The range accumulation of the 90-degree ray across Layer I, from 67.1 m depth to a depth of 280 meters, is 2934 m. This is entered (in km) at the appropriate place in Table 1.

If a comparison is made between the values of  $m$  and  $v$  used here and those listed in Ref. 1, it will be noted that the following changes have been made:

Derivative	NRL Report 6123	In this Report
$m$	$11.7 \times 10^{-12}$	$19.0 \times 10^{-12}$ (Fig. 3)
$v$	$9.6 \times 10^{-13}$	$17.8 \times 10^{-13}$ (Fig. 4).

These derivatives cannot be determined from the data in hand with good precision. However, the values used in this report are considered to be the more manageable in that they have been read from smoothed plots, illustrated by the circled points on Figs. 3 and 4.

The  $2X(\theta_o)$  data in Table 1 and Fig. 1 are also plotted as curve "d(up) 1,2,4 single" in Fig. 5. The curve presents two emission angles for each value of the zone range between the minimum at 64.34 km for the 87.1-degree ray and the 65.85-km range for the 90-degree ray. It is to be remembered that the zone is a circular area drawn at the depth of the source 67.1 m below the surface. The lower branch of d(up) 1,2,4 single ends at 82.2 degrees, where it is cut off by the sea bottom. The abrupt end of the upper branch at point E is a consequence of the restriction to the half-space below the source.

Up to this point the focus of interest has been kept on the 90-degree principal convergence fan  $\beta_o$  (Fig. 2) ejected into the lower half-space. A major deficiency in the predicted zone signal comes to light when these, the principal convergence rays alone, are used to calculate the zone radiation. Field observation indicates that rays other than those in fan  $\beta_o$  may be contributing to the zone signals. The deficiency is partly removed by the inclusion of rays which are ejected upward into the 67.1-m-thick layer of water

\*The symbolism associated with the curves in Fig. 5 will be explained later.

CONFIDENTIAL

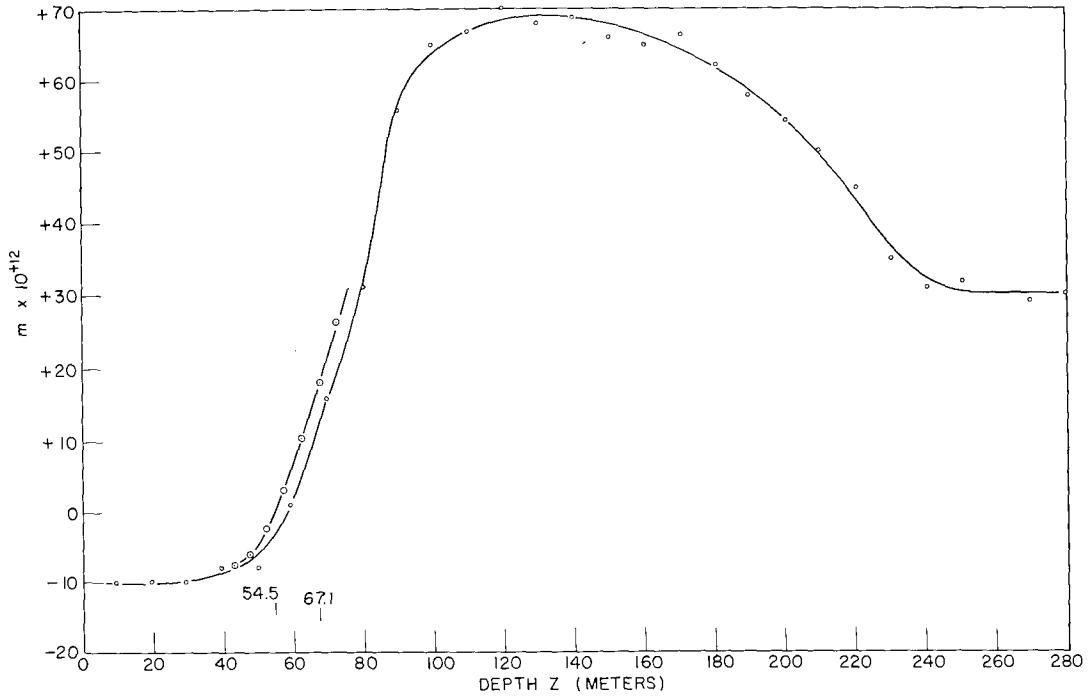


Fig. 3 - First derivative  $m$  of the function  $\eta^2(z)$  plotted vs depth. The data are for shallow depths (Layer I).

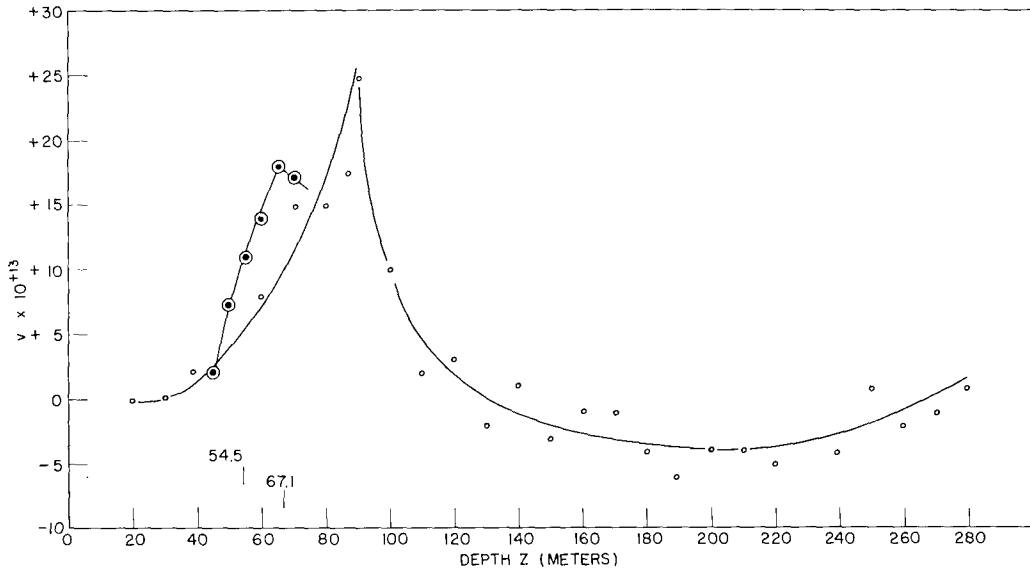


Fig. 4 - Second derivative  $v$  of the function  $\eta^2(z)$  plotted vs depth. The data are for shallow depths (Layer I).

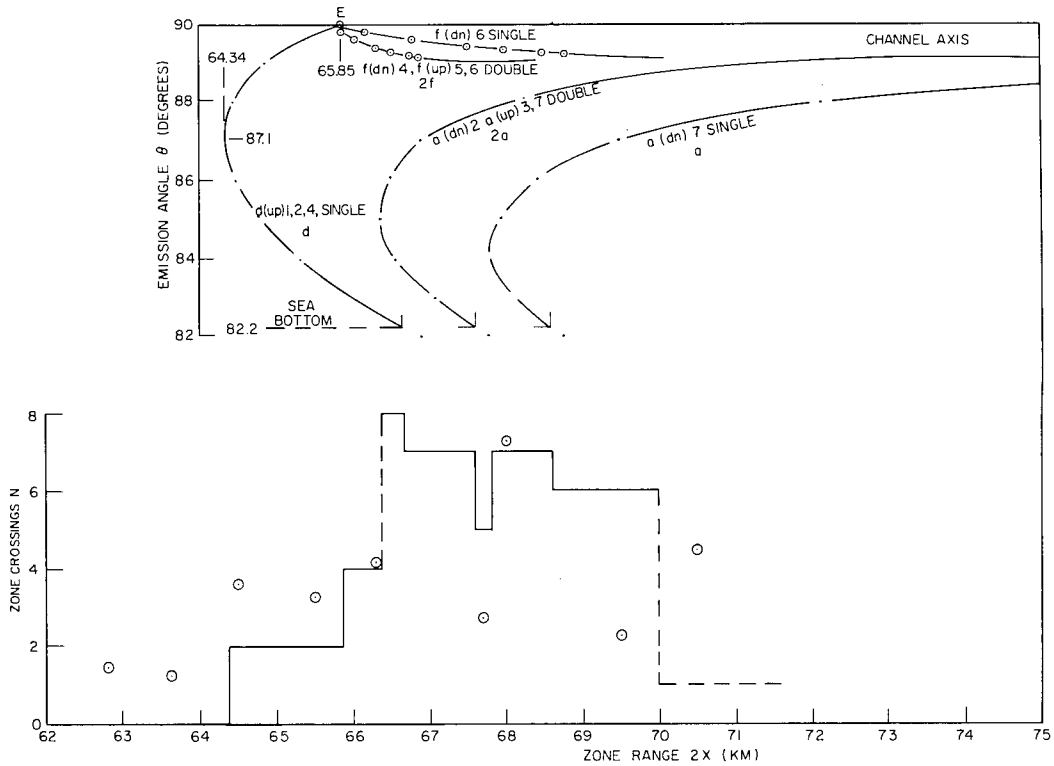


Fig. 5 - Emission angle  $\theta_0$  vs zone range  $2x$  for rays  $d$ ,  $f$ , and  $a$  of Fig. 2; also, the number of ray crossings  $N$  of a given zone is plotted vs the zone range  $2x$

between the source and the ocean surface. These rays eventually return to deep convergence paths after reflection or refraction in the 67.1-m layer near the source or near the zone.

The refraction conditions in the 67.1-m layer, Fig. 6, determine the manner in which rays initially ejected upward (fans  $a$  and  $f$ , Fig. 7) are returned near the source to the half-space below the source where they are subsequently refracted to the zone. Figure 5 is constructed to facilitate the counting of rays passing through each zone point. Each fan of contributing rays is represented by one of the curves, e.g., curve  $d(\text{up})$  1,2,4 single represents the principal convergence fan which is passing upward at the zone and is 2.30 km wide ( $66.64 \text{ km} - 64.34 \text{ km} = 2.30 \text{ km}$ ) in range extension and 7.8 degrees ( $90.0^\circ - 82.2^\circ = 7.8^\circ$ ) in angular width.

An important characteristic of the 67.1-m layer is the fact that the  $\eta^2(z)$  function has a minimum at  $z = 54.5 \text{ m}$ , Fig. 6, where  $m$  (Fig. 3), the slope of the  $\eta^2(z)$  function, is zero. In Fig. 3, circles mark the points which were read from the large-scale plot, in Fig. 6. Figure 6 is a plot of  $\eta^2(z)$  near  $z = 54.5 \text{ m}$ . The circles in Fig. 3 represent the values of  $m$  after interpolation and smoothing of the data in a depth region where a sufficiently fine-grained measurement of  $c(z)$  was not possible with the methods at hand. The other points are plotted from the first differences in Table 1 of Ref. 1 in the column headed  $m \times 10^{12}$ . Smoothing of the data presumes that the  $c(z)$  function itself is smooth. The presumption then is that  $\eta^2(z)$  is smooth. In taking second differences on the actual refraction measurement of  $\eta^2(z)$  without smoothing, the resulting scatter is so great as to render the required second derivative  $v = (d^2/dz^2)(\eta^2)$  (Fig. 4) marginal in computation. In Fig. 4 the circled points represent values of  $v$  after smoothing of the  $m$  values.

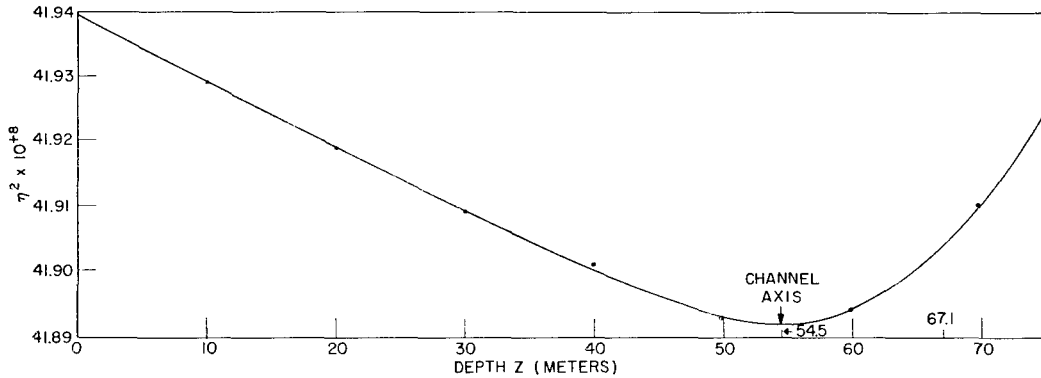


Fig. 6 - Plot of the refraction function  $\eta^2(z)$  for shallow depths (Layer I)

The behavior of a ray which has a vertex where  $m = 0$  was described in Ref. 1 using a parabolic approximation to the ray in the depth range where  $\eta^2(z) = mz + \text{constant}$ . It was shown that the value of  $z$  (54.5 m) for which the slope  $m = 0$  designates the axis of a "sound channel" or a "sound shadow," depending upon whether the second derivative  $v$  of  $\eta^2(z)$  at 54.5 m is negative or positive (Fig. 4). The value of  $v$  is about  $11 \times 10^{-13}$  at  $z = 54.5$  m. The ray of smallest grazing angle (angle from  $x$ ) issuing from the source at  $z = 67.1$  m has  $\theta_o = 90$  degrees and its vertex is at the origin. This ray is the lower border of the fan  $\beta_1$ , or  $f$ , in Fig. 2, as well as the upper border of fan  $\beta_o$  in Fig. 2. The upper border of fan  $\beta_1$  in Fig. 2 appears to be the ray whose vertex is on the  $z = 54.5$ -m axis at an as-yet-undetermined range  $X$  and whose emission angle is  $(\pi/2) + \beta_1$ . The vertex range  $X$  of this  $\beta_1$  border ray will later be shown to lie at infinity. Ray fan  $\beta_1$  is ejected into the thin layer (12.6 m thick) between 67.1 m and 54.5 m. In this layer  $\eta^2(z)$  is considered to be smooth (Fig. 6) so that the rays in the  $\beta_1$  fan can be computed. The smoothness of the  $\eta^2(z)$  function was manufactured simply by drawing the smooth curve through the points shown. These points in turn were deduced from a smooth reproduction of the  $T(z)$  function drawn by the 900-ft bathythermograph. The fan boundary, ray  $\beta_1$ , is the ray which appears to be horizontal (at  $z = 54.5$  m) for its vertex at this depth is at an infinite range. Rays of greater angle  $\theta_o$  such as  $r$ , Fig. 2, proceed across the axis to the water surface to  $R_a$  where reflection takes place. Rays  $g$  of lesser angle of emission have concave downward vertices at depths below the 54.5-m axis. The emission angle  $(\pi/2) + \beta_1$  of the boundary ray  $\beta_1$  can be determined from the fact that at a ray vertex the ray constraint  $p$  is equal to  $\eta(Z)$ . At the source the same number  $p$  is given by  $p = \eta(z_o) \sin(\beta_1 + \pi/2)$ . From these relations  $\beta_1 = \cos^{-1}[\eta(Z)/\eta(z_o)]$ . The best estimates of the border ray end values of  $\eta^2$  taken from  $\eta^2$  plots are

$$\begin{aligned} z_o &= 67.1 \text{ m} & \eta^2(z_o) &= 0.41904 \times 10^{-6} \\ z &= 54.5 \text{ m} & \eta^2(Z) &= 0.41892 \times 10^{-6}. \end{aligned}$$

The angle  $\beta_1$ , when the  $\eta^2$  values are inserted, is given by

$$\beta_1 = \cos^{-1} \sqrt{\frac{41.892}{41.904}} = 0.969 \text{ degree}.$$

The computation above is based upon a selection of ray constraint which will have such a value as to make the ray horizontal at  $z = 54.5$  m, i.e., have a first (upper) vertex at 54.5 m, but it does not indicate the direction of turning of the ray tangent through the vertex at the  $z = 54.5$ -m level. It is especially necessary in the present case where infinities are implied that the nature of the ray beyond the vertex point be examined.

UNCLASSIFIED

New computations based upon refraction parameters at the vertex must be initiated, with the value of  $x$  beyond the vertex to be found. All rays in the thin fan  $\beta_1$  of 0.969-degree angular width are concave downward. Each ray has an upper vertex. The first ray with  $\theta_o = 90$  degrees has its vertex at  $z = 67.1$  m,  $x = 0$ . At the other border where  $\beta_1 = 0.969$  degree, the vertex recedes to  $x = \infty$  at the level  $z = 54.5$  m. On the argument of symmetry it may be said that each ray in  $\beta_1$ , after passing through its vertex, turns downward and crosses the source plane  $z = 67.1$  m at  $x = 2X$  and enters the lower half-space with a grazing angle equal to its source grazing angle. Therefore, fan  $\beta_1$  contributes to convergence paths a very thin fan between  $\theta_o = 90$  degrees and  $\theta_o = (90^\circ - 0.969^\circ$  or  $89.031$  degrees), Fig. 2. The rays, however, enter the lower half-space at  $2X$  intervals spread out from  $X = 0$  to  $2X = \infty$ . The fan is far removed from the 87.1-degree angle of the principal convergence minimum.

For a short depth range  $h$  in the neighborhood of a given vertex level  $z_a$ , the approximation  $\eta^2(z) = \eta^2(Z_a) + m_a h + \frac{v_a}{2} h^2$  may be used to give the range accumulation  $x$  beyond  $x_a$  in the form of Eq. (2). This expression contains the first derivative  $m$  and the second derivative  $v$  of the function  $\eta^2$  at the vertex point  $Z_a$ . Both  $m$  and  $v$  are positive and finite at depths greater than  $z = 54.5$  m where  $h$  is small and positive. If the vertex is chosen successively closer to  $z = 54.5$  m, the refraction conditions in the ocean are such that the slope  $m$  decreases toward zero (Fig. 6), finally reaching a value such that  $2m/v \ll h$ . The range accumulation is then given approximately by

$$x_2 \approx p \sqrt{\frac{2}{v}} \ln \left[ \frac{v}{m} (2h) \right] \quad (3)$$

In Fig. 6,  $v$  is not zero at 54.5 m. When the vertex is taken to be very near to  $z = 54.5$  m, where the slope  $m$  is zero, and  $h$ , the independent variable of the ray function  $x(h)$ , is held fixed at a small value, the range accumulation, because of inverse dependence on the parameter  $m$ , increases without limit along  $b$ . This ray, Fig. 7, can reach the zone by travelling just below 54.5 m with slight concave downward curvature, entirely within the 12.6-m layer. The limiting ray on the axis between  $b$  and  $d'$ , Fig. 7, has a vertex at long range. Within this range rays can reach the zone and yet remain the 12.6-m layer.

In Eq. (3) positive (downward) values of the independent variable  $h$  were chosen for analysis. In consequence, the ray  $b$  passing close below  $z = 54.5$  m turns downward from its vertex. When negative values of  $h$  are chosen, in order to apply Eq. (3) to the layer above 54.5 m it must be remembered that in passing upward across the  $z = 54.5$ -m level the sign of  $m$ , Fig. 6, changes to a negative value. The result is that  $h/m$  remains positive on both sides of  $z = 54.5$  m and  $x_2$  increases as a positive real number immediately above that level, as well as immediately below it; the quantity  $2m/v$  remains  $\ll h$ .

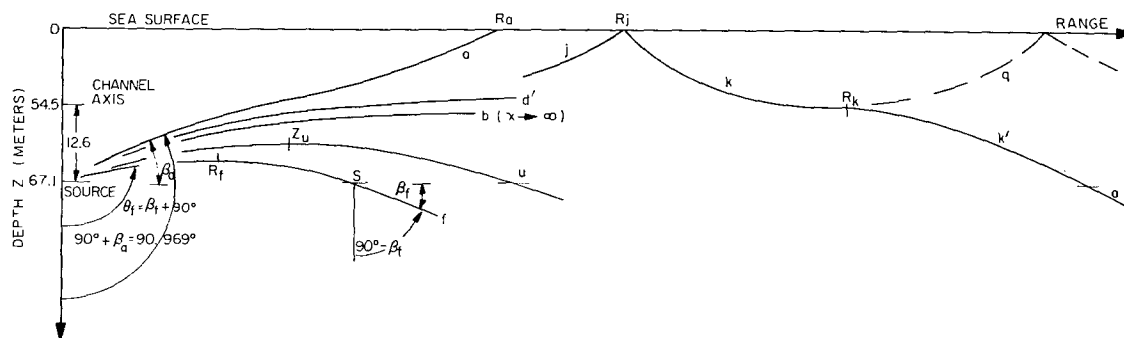


Fig. 7 - Depth  $z$  vs range  $x$  for typical refracted  $f$ -rays emitted at the source between  $90$  and  $90.969$  degrees

It appears now that two fans other than the 90-degree convergence fan are able to enter the lower half-space and to contribute to zone radiation via deep convergence refraction paths. They are designated by their typical rays  $f$  and  $a$  in Figs. 2 and 7. The whole  $f$ -fan of only one degree width is bent downward to enter the lower half-space at all ranges such as  $s$ , Fig. 2, from  $x = 0$  to  $x = \infty$ . In doing so, however, its grazing angles of entry extend from zero degrees, for  $\theta_o = 90$  degrees, to a maximum of  $\beta_1$  as  $x \rightarrow \infty$ .

The  $a$ -fan originates at the source between  $\theta_o = 90.969$  degrees and  $\theta_o = 180$  degrees, Figs. 2 and 8. All rays in this fan reflect once at the surface  $R_a$  and return to enter the lower half-space at all grazing angles between 0.969 and 90 degrees and at all ranges  $\Delta x_a$  from zero to infinity. A special ray in the  $a$ -fan which is returned by reflection enters the lower half-space at an angle of  $\theta_o = 87.1$  degrees and a range of  $x = 2649$  m, Fig. 8. This number was arrived at by numerical integration based upon the shallow depth refraction data in Fig. 6. It agrees well with  $\Delta x_a$  computed from rectilinear rays. The range of entry  $w$ , Fig. 2, of the other rays in the  $a$ -fan may be computed either by numerical integration or approximately by simple trigonometry where rays are considered to be straight lines originating at the image  $I$ , Fig. 8, 67.1 m above the surface so that the source-to-image distance  $H = 134.2$  m. The range increment  $\Delta x_a$  of entry of any ray in fan  $a$  into the lower half-space is then described by the relation  $\Delta x_a = H \tan \theta_a = 134.2 \tan \theta_a$ , where  $\theta_a$  (Fig. 8) is the angle of  $a$ -ray entrance into the lower half-space and the rays in the 67.1-m layer are nearly straight. The distances  $\Delta x_a$  computed for the angular range  $75 < \theta_o < 90$  degrees, are plotted in Fig. 9. The increments  $\Delta x_a$ , when added to the principal convergence ranges, yield range values for drawing curves  $a(\text{up})3$ ,  $a(\text{up})7$ , etc., in Figs. 5 and 10. The complicated symbols will be explained later.

## RAY CHAINS

In the 54.5-m layer qualitative ray geometry suggests the possibility of repeated ray reflection at the sea surface so that acoustic signals may be carried to great distances along a ray chain such as  $j$ ,  $R_j$ ,  $k$ ,  $R_k$ ,  $q$  in Fig. 2. A close inspection of ray curvature leads to the conclusion that under the refraction conditions existing on October 27-28,

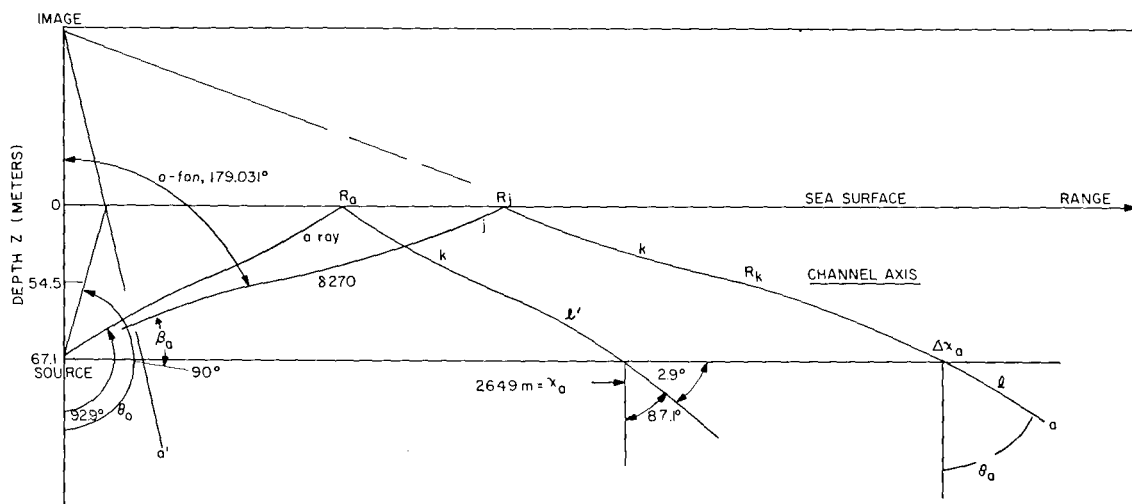


Fig. 8 - Depth  $z$  vs range  $x$  for typical reflected  $a$ -rays emitted at the source between 90.969 and 180 degrees

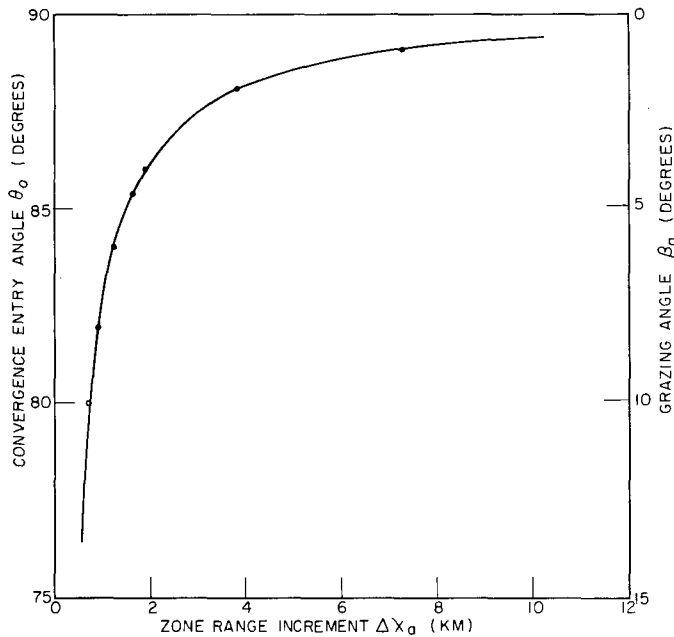


Fig. 9 - Zone range increments  $\Delta x_a$  vs convergence entry angle  $\theta_0$  for a-rays entering the lower half-space below the source. The angle  $\beta_a (= \pi/2 - \theta_a)$  defines the grazing angle of the a-ray.

1960 (Fig. 6), such chain rays cannot be formed and only one reflection, the first, from point  $R_j$  at the surface (Fig. 2) is possible. After reflection at  $R_j$  the signal is guided into the depths by the rays  $k$  and  $l$ , Fig. 2 or Fig. 8. The argument is based upon ray curvature.

The curvature of a plane curve is defined as  $\kappa = d\theta/ds$ , which is the rate of change of the curve's tangent angle  $\theta$  with distance  $s$  along the arc of the curve (ray). A sign may be ascribed to the curvature if care is exercised in being consistent with the geometry. The disturbing element is the use of  $z$  as positive downward. The situation becomes clear if definitions are guided by Fig. 11. The ray segment  $R$  is drawn in the second quadrant. The definitions and sign conventions used in this report are listed below as they apply to Fig. 11:

- $s$  increases positively from left to right, i.e., in the direction of increasing  $x$
- $\theta$  is the slope angle, measured from the plumb line
- $\theta$  and  $d\theta$  are positive for counterclockwise rotation of the ray tangent
- $z$  is positive downward parallel to the plumb line
- $\kappa$  bears the sign of  $d\theta$ .

To put the curvature in a form useful here, the following three relations are needed:

- a. The definition of curvature is  $\kappa = d\theta/ds$ .
- b. The differential triangle is  $ds^2 = dx^2 + dz^2$ .

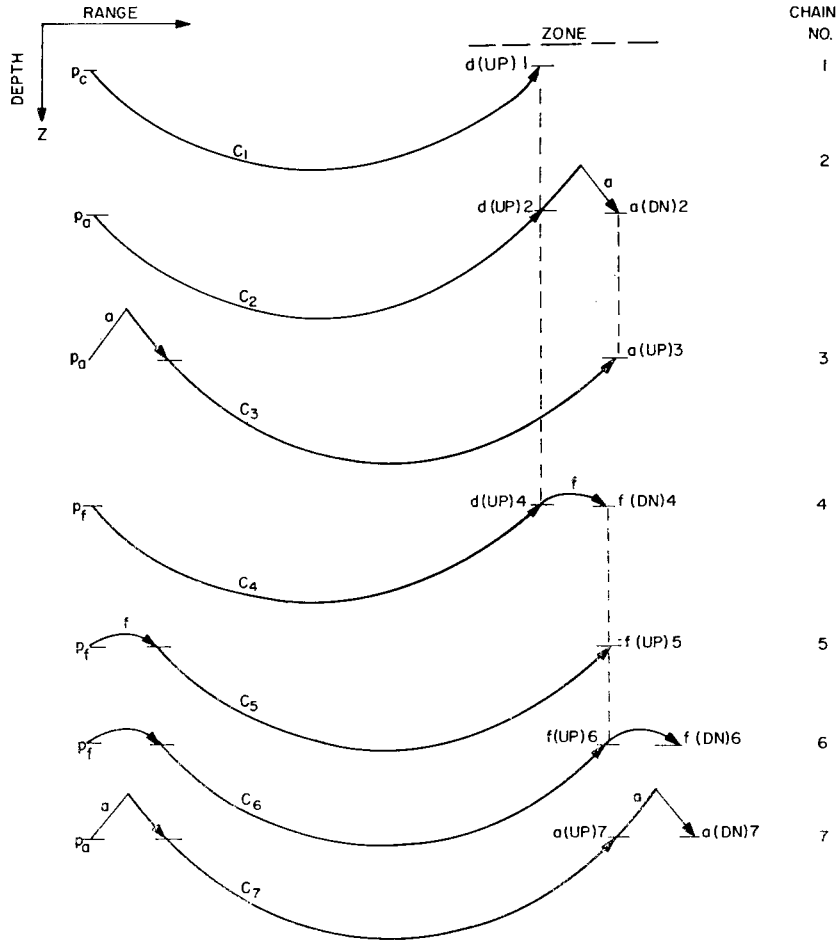


Fig. 10 - Depth-range characteristics of ray chains made up of ray segments a, d, and f

c. Snell's law in terms of the ray constraint  $p$  is  $p = \eta \sin \theta$ .

When the arc element  $ds$  is drawn in the second quadrant, Fig. 11,  $ds = dz \sec \theta$ . The variation  $dp$  in the ray constraint along the ray is zero, so that  $\eta \cos \theta d\theta + d\eta \sin \theta = 0$ . From this relation the variation in angle is given by  $d\theta = -(d\eta/\eta) \tan \theta$ . When the ratio  $d\theta/ds$  is formed and the  $\eta^2$  value is used as dependent variable, the curvature becomes

$$\kappa = - \frac{d\eta^2}{dz} \frac{p}{2\eta^3} = - m \frac{p}{2\eta^3} \tag{4}$$

An alternative expression  $\kappa = p \, dc/dz$  follows from the introduction of the identity  $\eta c = 1$ . The curvature of the ray at any point is now expressed in Eq. (4) in terms of the slope  $m$  of the function  $\eta^2$ , Fig. 6. The sign of the slope  $m$  is opposite to the sign of the curvature. The refraction parameter  $\eta^2$  (or  $\eta$ ) is always positive, finite, and not zero. It is a function of  $z$  only. The ray constraint  $p$  is constant along a chosen ray and is positive for all rays because the limitation on  $\theta$  is  $0 < \theta < \pi$ .

The rays whose curvature will be described are drawn in Figs. 7 and 8, which depict the 67.1-m surface layer. This layer is subdivided into two thinner layers, one 54.5 m

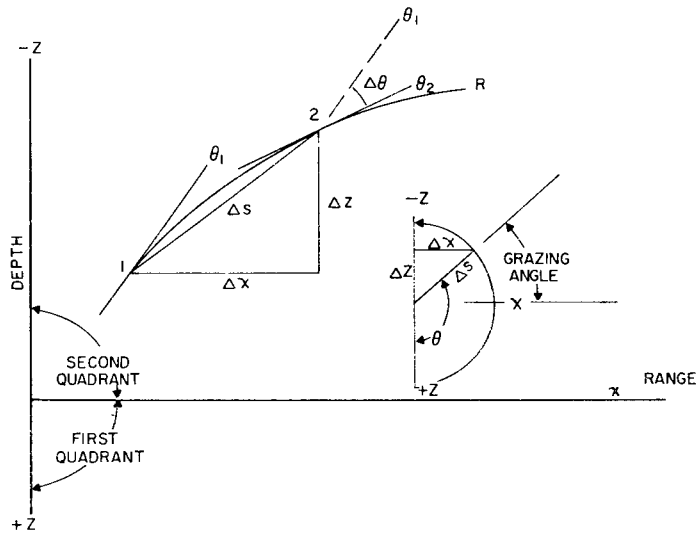


Fig. 11 - Ray curvature geometry

thick, the other 12.6 m thick, by the plane located at the refraction axis at 54.5 m depth. Four rays,  $f$ ,  $b$ ,  $d'$ , and  $a$  (Fig. 7), emanate from the source into the 12.6-m layer. These rays will be used to illustrate curvature as governed by the sign of  $m$ , Fig. 3. Ray  $f$  has its vertex at a depth greater than the refraction axis, where  $m$  (Fig. 3) is positive. The curvature is therefore negative and  $f$  is concave downward along its entire course in the 12.6-m layer; its tangent turns clockwise (negative direction) along the course of the ray. Ray  $b$ , remaining always above  $f$ , Fig. 7, rises from the source towards its own vertex point at a depth approaching 54.5 m, but at a range  $x$  approaching an infinite distance. Except for the indeterminate vertex point at infinity, ray  $b$  is entirely within the positive  $m$  region and is therefore concave downward along its entire course. Its curvature is negative but approaches zero as  $m \rightarrow 0$ . This happens when  $z \rightarrow 54.5$  m, Figs. 6 and 3.

Ray  $d'$ , which is drawn across the refraction axis, is the counterpart of  $b$  in that it is so close to the axis as to continue in the upper 54.5-m layer to a very great range before positive curvature turns it up to the surface. It has positive curvature because  $m$  is negative at depths less than 54.5 m, Fig. 6. If  $\theta_0$ ,  $m$ , and the zone range  $2X$  are right, ray  $d'$  reflects in the sea surface near  $X$ , the half zone range, then it passes downward to the zone. The curvature of  $d'$  below the refraction axis is negative ( $m$  is positive), but above the axis the curvature is positive. On the axis where  $m = 0$ , the curvature is zero. Rays, when crossing the axis, have no curvature and the crossing point is a point of inflection. Rays  $d'$ , Fig. 7, which succeed in crossing the axis upward will have, on arguments of symmetry, such a value of  $p$  as to cross the axis downward after being reflected at the surface. There are no rays issuing from the surface reflection point with the proper value of  $p$  to permit an upward turning at the axis, such as shown at  $R_k$  for the fictitious ray  $q$  in Fig. 7. The rays which turn downward and remain below the axis, such as  $f$  and  $k'$ , Fig. 7, enter the lower half-space and reach the zone by entering the convergence fans. The rays which travel to the zone wholly within the 67.1-m layer reach the zone in elapsed times characteristic of channel sound speed. The time is generally sufficiently shorter than times by way of convergence to permit a clear separation of channel and convergence pulses on the field recorder.

Two rays in the  $f$ -fan are marked  $s$  and  $u$  where they enter the lower half-space, Fig. 7. One has its vertex at  $R_f$  and the other at  $Z_u$ . The entry ranges  $s$  and  $u$ , also called  $f$ -increments or  $\Delta x_f$ , required for zone crossing estimates were computed by use

of Eq. (2) into which appropriate values of the parameters  $p$ ,  $v$  and  $m$  were inserted. Results are listed in Table 2. For ease of table consultation the grazing angles  $\beta_f = 90^\circ - \theta_f$ , Fig. 7, are used and  $\sin \theta_o = \cos \beta_f$ . The fan of  $f$ -rays is only about 1 degree wide. Only a few angles need be used. The first step is to distribute the chosen grazing angles  $\beta_f$  over this narrow range (column 1, Table 2). Column 2 contains the angle  $\theta_f$  of entry into the lower half-space. This is also equal to the angle  $\theta_o$  in the function  $2X(\theta_o)$  which heads columns 3-5. The convergence range  $2X(\theta_o)$  is listed as read from Fig. 1 at the angles  $\theta_o$  given in column 2. In column 6 the  $f$ -range increments  $\Delta x_f$  as computed from Eq. (2) are listed. Parameters  $m$  and  $v$  were read from Figs. 3 and 4 at  $z$  values appropriate for the vertex values for the listed  $f$ -ray angles  $\theta_o$ . The ray constraint  $p$  is equal to  $\eta_o \sin \theta_o$  at the source ( $z = 67.1$  m) and is known for any ray as soon as its angle  $\theta_o$  is chosen. The vertex depth  $Z$  for the ray can then be determined from Fig. 6 for  $p^2 = \eta^2(Z)$ . The range accumulation  $x_2$  computed by use of Eq. (2) yields the horizontal distance from  $R_f$  to  $s$  on ray  $f$ , Fig. 7. The integration starts at the vertex  $R_f$  and extends downward in the positive  $z$  direction for a positive distance  $h = z_o - Z$ , ending at the source level  $z_o = 67.1$  m. By symmetry of the ray arc the whole range accumulation of the  $f$ -ray in the 12.6-m channel is seen to be  $2x_2$ , and  $2x_2$  is called an  $x$  increment in the ray chain. Consequently,  $2x_2$  is listed in Table 2 as  $\Delta x_f$  and plotted against  $\theta_f$  in Fig. 12. From the smooth curve drawn through the computed points, Fig. 12, intermediate  $\Delta x_f$  values can be read which, when added to zone ranges for the corresponding  $\theta_o = \theta_f$  angles on the main convergence function  $d(\text{up})1,2,4$  single of Figs. 5 and 1, yield four new convergence rays (circled points at top of Fig. 5) for the  $f$ -fan. These rays are  $f(\text{dn})4$ ,  $f(\text{up})5,6$  double, and  $f(\text{dn})6$  single on Figs. 5 and 10. Columns 4 and 5 in Table 2 yield the zone ranges for these four  $f$ -rays which enter the convergence depths. Their two convergence functions, Fig. 5, are also formed by circled points at the top of the figure. One is double and the other is single. The double form contributes two zone crossings; the single function contributes one zone crossing. The total zone crossings for the  $f$ -functions is therefore three.

The computations yield the range increments for the entry of six rays from the 67.1-m layer into the lower half-space. The whole range at the zone for each ray in the  $f$ -fan is the sum of the range accumulation  $\Delta x_f$ , Table 2, in the 12.6-m layer for that ray and the accumulation  $2X(\theta_o)$  along a convergence ray path while in the lower half-space for the same ray.

The build up of acoustic energy at the zone is accounted for by the demonstration that a number of fronts are superimposed upon each other at a zone point. The foregoing

Table 2  
Zone Ranges and Range Increments for  $d$ - and  $f$ -Fan Rays

Grazing Angle $\beta_f$ (degree)	Entry Angle $\theta_f = 90^\circ - \beta_f$ (degrees)	Range Accumulation to Convergence Zone (km)			Range Increments
		$d(\text{up})1,2,4$ single [= $2X(\theta_o)$ ]	$f(\text{dn})6$ single [= $2X(\theta_o) + 2\Delta x_f$ ]	$f(\text{up})5,6$ $f(\text{dn})4$ double [= $2X(\theta_o) + \Delta x_f$ ]	$\Delta x_f$ (km)
0	90	65.86	65.86	65.86	0.0
0.2	89.8	65.52	66.16	65.84	0.32
0.4	89.6	65.30	66.74	66.02	0.72
0.6	89.4	65.10	67.50	66.30	1.20
0.7	89.3	65.05	67.97	66.51	1.46
0.8	89.2	65.00	68.48	66.74	1.74
0.85	89.15	64.95	68.73	66.84	1.89

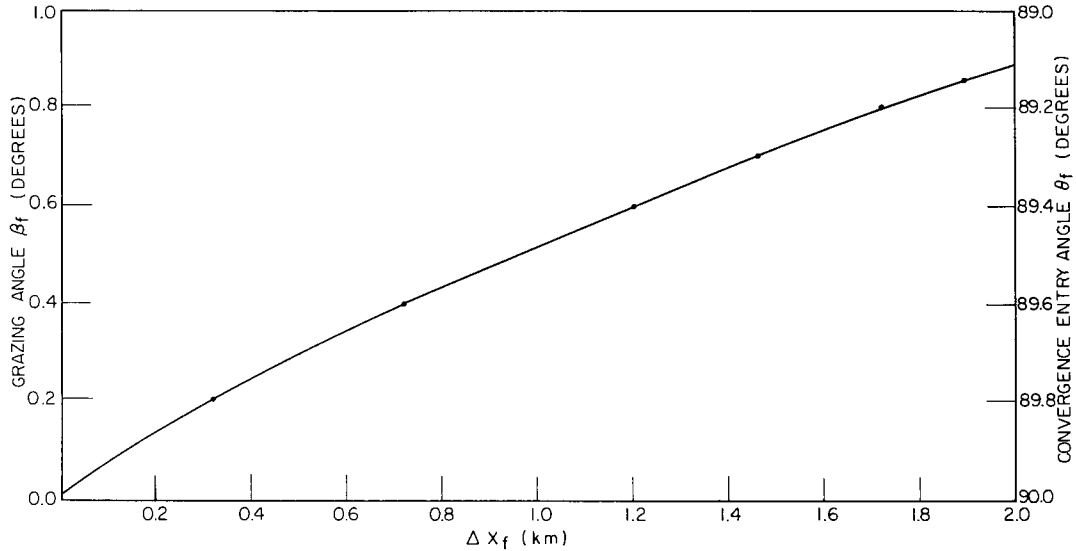


Fig. 12 - Zone range increment  $\Delta x_f$  vs grazing angle  $\beta_f$  and convergence entry angle  $\theta_f (= 90^\circ - \beta_f)$  for f-rays

analysis leads to the conclusion that seven ray chains are involved. These are sketched (not to scale) in Fig. 10 and are separated so as to bring out their essential character. The convergence link which covers the greater part of the range is designated  $c_1 \dots c_7$  in Fig. 10. The letters a and f indicate that rays are part of the a- or f-fans and that chain segments a or f are to be added. Each ray starts, at the source, with its separate source angle  $\theta_o$  and ray constraint  $\rho$ . The ray constraint remains fixed throughout the length of the ray (or ray chain). The ray crosses the zone either in an upward or downward direction as indicated by the arrowheads. Ray chain number 1, Fig. 10, of constraint  $\rho_c$  passes to the zone along the convergence path  $c_1$  without additions. Ray chains number 2, 3, and 7 of constraint  $\rho_a$  have a short starting or ending segment of the a-fan where the reflected ray is approximately rectilinear in the channel. Ray chains 4, 5, and 6 of constraint  $\rho_f$  have f-fan refraction segments. The last two ray chains No. 6 of constraint  $\rho_f$  and No. 7 of constraint  $\rho_a$ , have two surface channel added segments. One f-segment is added to the convergence link near the source, and another near the zone in chain No. 6. In chain No. 7, a-fan segments are similarly added. There is no ray chain having an f-segment at one end and a-segment at the other because  $\rho$  must be continuous, i.e.,  $\rho_f \neq \rho_a$ . Around each of the seven ray chains drawn in Fig. 10 there is a fan of similar ray chains which spread across the zone and overlap there for a range distance determined by the angular width of the fan and the length of the pulse.

Quantitative addition of acoustic pressures cannot be determined solely from Fig. 10. The  $2X(\theta_o)$  functions of Fig. 5 are presented for this purpose. Figure 10 is used for counting the number of rays passing either up or down through a selected zone point. The principal convergence fan of rays, of which  $c_1$ , Fig. 10, is one, is represented in Fig. 5 by the function  $2X(\theta_o)$  marked d(up)1,2,4 single. The numbers indicate the pertinent convergence links in Fig. 10. Other  $2X(\theta_o)$  values are constructed by adding the a- or f-range increments to the convergence ray links  $c_2, \dots, c_7$  in Fig. 10.

Before construction of the  $2X(\theta_o)$  functions in Fig. 5 can be completed with confidence, it is essential that the ray chains which pass through a zone point be identified. This, at the risk of some repetition, requires continued discussion of the ray chains in Fig. 10 and crossings in Fig. 5. Construction of the  $2X(\theta_o)$  functions can be done only in case of relatively simple refraction conditions which have enough temporal life to make

the effort worthwhile. In the present case only three regions of refraction and one of reflection have been identified. These lead to identification of the seven typical ray chains in Fig. 10. Each is characterized by one of the three ray constraints  $p_c$ ,  $p_a$ , or  $p_f$ . Each chain consists of a principal convergence link  $c$ , to the ends of which shallow channel links  $f$  or  $a$  may be added. All of the convergence links  $c_1 \dots c_7$  end with (up) arrows. Three of the  $c$  arrows (links 1, 2, and 4, Fig. 10) are marked  $d(\text{up})1$ ,  $d(\text{up})2$ , and  $d(\text{up})4$ . This means that the  $d(\text{up})$  crossings are represented by  $d(\text{up})1,2,4$  single, Fig. 5. These links are rays in the principal convergence fan, all rays of which start from the source without initial increments in  $f$  or  $a$ . The  $2X(\theta_o)$  function  $d(\text{up})1,2,4$  single, Fig. 5, is not subject to doubling. Only one zone crossing is represented by the three  $2X(\theta_o)$  values because all three rays have a common origin and represent one wave front and there is no  $d$ -down ray.

Ray chains 2 and 3 have the same  $x$  length. Number 2 ends with an  $a$ -segment whereas No. 3 starts with an  $a$ -segment. The range accumulations to the chain ends are identical and their ray constraints  $p_a$  are identical, but the rays themselves cannot be superimposed. They do not represent one and the same front because No. 2 ends with the down crossing  $a(\text{dn})2$  and No. 3 ends with an up crossing  $a(\text{up})3$ . These occur at the same range. Number 2 enters convergence space at the source with  $\theta_o$  appropriate for  $p_a$ , but the other chain, No. 3, travels the reflection path  $a$  before it too enters convergence space with constraint  $p_a$ , also at angle of entry  $\theta_o$ . Each point on the  $2X(\theta_o)$  curve, Fig. 5, for chains No. 2 and No. 3 in Fig. 10 represents two zone crossings at each range; one  $a(\text{dn})2$ , the other  $a(\text{up})3$ . The curve is consequently labeled "double" in Fig. 5 and the velocity potential at the zone point is doubled, i.e., twice the value of the velocity potential of one ray. A similar situation obtains with ray chains 4 and 5. Here the end links are of the  $f$  variety. The double crossing is represented by  $f(\text{dn})4$  and  $f(\text{up})5$  arrows occurring at one and the same range. The corresponding  $2X(\theta_o)$  curve is designated  $f(\text{dn})4$  and  $f(\text{up})5,6$  double, in Fig. 5. The  $f(\text{up})5$ , and  $f(\text{up})6$  are equivalent to but one crossing. When identical increments are added to both ends, chains such as No. 6 and No. 7, Fig. 10, lead to the single curves  $f(\text{dn})6$  and  $a(\text{dn})7$  of Fig. 5.

Two up crossings,  $f(\text{up})6$  and  $a(\text{up})7$ , remain to be described. At first sight these appear to give rise to new  $2X(\theta_o)$  curves by doubling. This, however, is not the case. Although  $f(\text{up})6$  has the same range as  $f(\text{up})5$ , each is not a separate ray chain representative of a separate front. Chains 5 and 6 are identical up to  $f(\text{up})5$  and  $f(\text{up})6$  where they represent one and the same front and count as one and the same crossing. It is for these reasons that there is no separate curve in Fig. 5 labeled  $f(\text{up})6$ . The same situation obtains when chains 3 and 7 are compared. The crossings  $a(\text{up})3$  and  $a(\text{up})7$  are counted as one and  $a(\text{up})7$  is omitted as a separate curve in Fig. 5.

The group of points in the narrow angle between  $\theta_o = 89$  and  $90$  degrees in Fig. 5 represents the zone ranges for ray chains wherein the  $f$ -fan contributes range increments to be added to the principal convergence link. Similarly, the two curves on Fig. 5 are constructed from the  $a$ -ray links and the convergence link.

Returning again to the  $f$ -fan data in Table 2 numerical examples will be discussed. In column 5 one  $\Delta x_f$  increment is added to  $2X(\theta_o)$  to give the range of the ray chains which have but one  $f$ -segment such as No. 4 and No. 5, Fig. 10. The No. 4 chain ends with a down arrow. The No. 5 chain ends with an up arrow. The two chains have identical ranges and  $p_f$  values but represent two separate fronts. The corresponding curve in Fig. 5 is marked  $f(\text{dn})4$  and  $f(\text{up})5,6$  double. The crossings are double because both down and up crossings occur. The  $f(\text{up})6$  does not contribute a new front. The convergence link  $c_4$ , Fig. 10, has the  $d(\text{up})4$  arrow. The range of this arrow is a point on the main convergence  $d(\text{up})1,2,4$  single curve, Fig. 5. It appears in both columns 4 and 5 when  $\Delta x_f = 0$  at  $\theta_o = 90$  degrees. The main convergence curve  $d(\text{up})1,2,4$  single and the  $f$  curves all join at the point E, Fig. 5, where  $\theta_o = 90$  degrees,  $2X(\theta_o) = 65.86$  km, and  $\Delta x_f = 0$ . In ray chain No. 6, Fig. 10, two  $\Delta x_f$  increments are added, one near the source,

one near the zone. These are added to the appropriate convergence range in column 3, e.g.,  $65.52 + 2 \times 0.32 = 66.16$  km in column 4. The up arrow f(up)6 is already accounted for in the fan of ray chain No. 5. Doubling of crossings by superposition of the identical arrows in identical rays cannot be used to attain doubled sound pressures. Doubling of this kind degenerates to the representation of one ray and one pressure value. The  $2X(\theta_o)$  representation is then f(up)5,6 combined with f(dn)4 to make a double front curve. The f(dn)6 crossing of ray chain 6 (column 4, Table 2) is plotted in Fig. 5 as the f(dn)6 single curve.

The zone crossings in ray chains 2, 3, and 7, Fig. 10, in which the reflection process  $a$  appears are determined by a scheme similar to that by which the  $f$ -chain crossings were obtained, except for the fact that the  $x$  increment is computed differently. The pertinent numerical results are listed in Table 3. The angular width of the  $a$ -fan, i.e., the grazing angle  $\beta_a$ , Figs. 7 and 8, although larger than that of the  $f$ -fan, is still limited to about 8 degrees. The angle  $\beta_a$  is limited on the low side by the border ray  $\beta_a = 0.969$  degree ( $\theta_o = 90.969$  degrees), and on the high side by  $\theta_o = 180$  degrees ( $\theta_a = 0$  degree). The angle  $\theta_a$ , Fig. 8, is the ray angle of entry of the  $a$ -ray into the convergence half-space after reflection in the surface as represented by down crossings near the source. Rays represented by  $\beta_a > 8$  degrees,  $\theta_a < 82.2$  degrees are considered in this study to be lost in the sea bottom. Bottom acoustical phenomena form a wide area of investigation which cannot be entered into in this study.

The  $\beta_a$  fan is divided into seven intervals represented by the entries in column 1, Table 3. The corresponding  $\theta_a$  values are listed in column 2. The  $a$ -reflection range increments  $\Delta x_a$ , column 6, were read from Fig. 9. Accumulation of range  $2X(\theta_o)$  along the convergence links  $c_3$  and  $c_7$ , listed in column 3, were read from Fig. 1 for the angles  $\theta_a$ . The whole zone range for the a(dn)2 crossing chain 2, Fig. 10, and also the (equal) whole range for the a(up)3 chain 3 are listed in column 5. The  $2X(\theta_o)$  function for these two chains are plotted as one curve marked a(dn)2, a(up)3,7 double, Fig. 5. One  $\Delta x_a$  increment occurs near the source on chain No. 3; the other occurs at the zone on chain No. 2. Chains 2 and 3 are paired in the same way that chains 4 and 5 are paired, but the resulting  $2X(\theta_o)$  functions are much different. The final chain, No. 7, is made up of the  $x$  accumulation of the  $c_7$  link, to which are added the two  $a$ -type increments, one at each end. The range accumulation result (e.g., for the entry  $\beta_a = 1$  degree, the accumulation is  $64.84 + 2 \times 7.32 = 79.48$  km for Chain 7) is listed in column 4 under the heading

Table 3  
Zone Ranges and Range Increments for  $a$ -Fan Rays

Grazing Angle $\beta_a$ (degrees)	Entry Angle $\theta_a = 90^\circ - \beta_a$ (degrees)	Range Accumulation to Convergence Zone (km)			Range Increments
		d(up)1 [ $2X(\theta_o)$ ]	a(dn)7 single [ $= 2X(\theta_o) + 2\Delta x_a$ ]	a(dn)2 a(up)3 double [ $= 2X(\theta_o) + \Delta x_a$ ]	$\Delta x_a$ (km)
0.969	89.031	-	-	-	-
1	89	64.84	79.48	72.16	7.32
2	88	64.40	72.10	68.25	3.85
3	87	64.34	69.44	66.89	2.55
4	86	64.50	68.40	66.45	1.95
5	85	64.84	67.90	66.37	1.53
6	84	65.28	67.80	66.54	1.26
7	83	66.00	68.14	67.07	1.07
8	82	66.81	68.71	67.76	0.95

a(dn)7 single. The a(up)7 crossing on chain 7 is already accounted for in chain 3 and appears as the numeral 7 in the double a-curve, Fig. 5. Column 4 values, when plotted against  $\theta_a$ , yield the single curve a(dn)7 in Fig. 5.

The convergence fans are folded by the refraction peculiarities of the deep water so as to exhibit two up crossings through each range point in the zone if the fan has sufficient angular width. This fact is demonstrated by the two branches to the  $2X(\theta_o)$  functions in Fig. 5. If a vertical line is drawn through the d(up) curve at, say, 65 km it will cross the lower branch at  $\theta_o = 84.6$  degrees and the upper branch at 89.2 degrees. At 65 km, therefore, two rays pass upward through a single point. At this point the two acoustic velocity potentials add to give an enhanced acoustic intensity which is the classic convergence zone signal enhancement. In the event the upper layers return rays to the convergence region, these rays also contribute to zone signal enhancement. If the fan is narrow the  $2X(\theta_o)$  functions, such as f(up) and f(dn), may have but one branch.

The contribution of all rays can be estimated by counting the number of intersections of a zone range ordinate line with the several  $2X(\theta_o)$  functions plotted in Fig. 5. Each contributing ray is one of the infinitude of rays in each of seven ray fans. The seven ray fans designated by their Fig. 5 symbols are listed in Table 4. The abbreviated symbols in the 4th column, and written near the curves in Fig. 5, are introduced for the purpose of clarity in the immediately following discussion of Fig. 5.

Table 4  
Symbolism Associated with the Seven Ray Fans  
Which Define the Principal Convergence Zone

Number of Overlapping Fans*	Fan Name	Code (see Fig. 5)	Abbreviated Symbol (see Fig. 5)
1	Principal Convergence	d(up)1,2,4 single	d
2	One "a" surface reflection	a(dn)2; a(up)3,7 double	2a
1	Two "a" surface reflections	a(dn)7 single	a
2	One "f" refraction	f(dn)4; f(up)5,6 double	2f
1	Two "f" refraction	f(dn)6 single	f

\*Each fan constitutes an infinitude of rays.

## ZONE CROSSINGS

Along the bottom of Fig. 5 a stepped line is drawn. The location of any point on the line is specified by an ordinate value N, which is the number of separate fan functions  $2X(\theta_o)$  crossed by a chosen vertical line, and an abscissa which is the range  $2X$  at which the vertical line is located. When set at 64 km the vertical line crosses no fan function. It falls short of the minimum range 64.34 km of the curve d. The number of crossings is zero, as indicated by the lowest step, and therefore the zone radiation is judged to be zero. At 64.34 km the crossings increase suddenly to two because the vertical line intersects both branches of curve d. A crossing number of unity is infinitesimally close to the crossing of two. The curves cannot be separately identified. This circumstance is symbolized by the vertical rise of the step from zero to two. Crossings remain constant at two until the vertical is moved to 65.86 km where the f curves start and the upper branch of the d curve ends. At a small distance above 65.86 km an increment of three

crossings is added to the remaining one still in effect for the lower branch of d. Curve 2f contributes two crossings and curve f contributes one. The total height of the crossing line jumps by two units to four at 65.86 km. At 66.37 km the minimum range of the curve 2a is encountered, and the crossings jump by four units. The step curve of N is now at the eight crossing level which continues to 66.65 km where the lower branch of d is stopped by the bottom and the step curve drops to 7. The 7 level continues to 67.62 km where the lower branch of 2a is cut off by the bottom and the step curve drops by two units to 5. It rises again by two units to 7 at 67.8 km where the minimum range of a is encountered. The step curve continues at 7 until range 68.6 km is reached where it drops by one unit to 6 where the lower branch of a is stopped by the bottom. Thereafter the crossings apparently remain at 6 indefinitely.

The last sentence in the preceding paragraph raises doubts as to the interpretation of crossings when the  $2X(\theta_o)$  curves tend to coalesce, as they do along the line 89.031 degrees, Fig. 5, and at the point E where  $2X = 65.83$ . At point E where two  $2X(\theta_o)$  f curves meet, one of which is double, it would appear that the crossings would amount to four. Actually there is a single crossing at E. The three curves which meet there are d, f, and 2f. As the angles of entrance into the convergence paths  $c_1, c_2, c_4, c_5$ , and  $c_6$ , Fig. 10, increase toward 90 degrees, the rays become horizontal. The grazing angle  $\beta_f$ , Fig. 7, approaches zero and the f range increments  $\Delta x_f$ , Table 2, all approach zero. The five convergence links  $c_1, c_2, c_4, c_5$ , and  $c_6$  approach coincidence. The result is that at point E only one  $2X(\theta_o)$  function exists and the crossing is unity. As the grazing angle  $\beta_f$  rises from zero, the increment  $\Delta x_f$  increases toward infinity at  $\beta_f = 0.969$  degree, Fig. 7. The ranges on the f curves of Fig. 5 increase toward infinity as  $\beta_f \rightarrow 0.969$  degree, and the f increment attached to the far end of chain 4, Fig. 10, will continue as a ray in the channel above the source not returning as f(dn)4 to contribute to zone intensity. This reduces by one unit the crossings for one f curve at far ranges. Another unit decrease appears in the 5 chain because the f increment near the source has moved the whole convergence chain  $c_5$  outward toward infinity. Similarly,  $c_6$  is moved to infinity so that all three f contributions to zone intensity are lost at great ranges. This limit was arbitrarily set at 70 km, Fig. 5, where crossings then fall to three.

Increments  $\Delta x_a$  increase as the grazing angle  $\beta_a$ , Fig. 9, decreases and would become infinite if  $\beta_a$  were allowed to fall to zero. Its lower limit is  $\beta_a = 0.969$  degree. At this angle  $\theta_a = 89.030$  degrees and  $\Delta x_a = 7.95$  km. But this figure is erroneous because the formula for computation ( $\Delta x_a = 134.2 \tan \theta_a$ ) is now not a good approximation. Actually, at the border grazing angle 0.969 degree,  $\beta_a$  and  $\beta_f$  are equal and  $\Delta x_a$  increases without limit, just as  $\Delta x_f$  does when  $\beta_f \rightarrow 0.969$  degree. The arguments cited about ranges for  $\Delta x_f \rightarrow \infty$  are now applicable to large values of  $\Delta x_a$ . The a-chain link, Fig. 10, is now so long as to keep the rays out of convergence paths, and the a crossings also disappear beyond, say, 70 km. The crossings N consequently drop to zero, and the zone ends somewhere beyond 70 km, unless channel signals are mistaken for convergence signals. In this event N would drop to one at long ranges.

## WAVE TRANSMISSION THEORY

The foregoing writing has to do with the behavior of plane curves  $(x, z)$  whose shapes are determined by the constraint  $p = \sin \theta/c(z)$ . The slope angle is  $\theta$ , and  $c(z)$  is an empirically determined function of the depth  $z$ . No mention so far has been made of acoustic properties. So, before the distribution of crossings shown in Fig. 5 are reduced to numbers which can be compared with field measurements, it will be helpful to give a brief extension of the applicable theory.

Simple harmonic spherical waves expanding outward from a simple source in deep water can be described by the elementary velocity potential

$$\varphi = \frac{A}{r} e^{ik(ct-r)}$$

where  $r$  is the radial distance from the source,  $A$  is the amplitude of sinusoidally oscillating volume emission which crosses each unit of surface of the sphere  $r$  drawn around the source,  $c$  is the speed of sound,  $\lambda$  is the wavelength of the emitted sinusoidal wave of frequency  $f = c/\lambda$ , and  $k = 2\pi/\lambda$ . Under the conditions of the refraction situation described here the radii are not rectilinear, and  $c$  is not everywhere the same, it is assumed that the wave surfaces of constant  $\varphi$  are adequately described by the formula. The rays are the "ray paths" of sonar engineering. Pulses of sonar signal consisting of a limited number (packet) of sinusoidal wave fronts follow the ray paths. Under the refraction and reflection conditions in the acoustic field, it is possible for more than one ray (i.e., one wave front) to pass through a point in the field at the same time, each front being separately described by  $\varphi_n$  the elementary formula for the velocity potential of the  $n$ th wave. At the zone, each of the crossings represent the passage of one ray through the zone point  $x_n$ , and the velocity potential for the  $n$ th ray is

$$\varphi_n = \frac{A}{r_n} e^{ik(ct-r_n)}.$$

The total potential for  $N$  fronts at that point is then given by

$$\varphi_Z = \sum_{n=1}^N \varphi_n.$$

But this presumes that each of the  $N$  fronts is a train of fronts of sufficient length to overlap, either completely or partially, at a zone point  $x$ . The potential  $\varphi_Z$  may be expressed in terms of the velocity potential  $\varphi_m$  associated with the one ray  $r_m$  emanating from the source at 87.1 degrees and intersecting the zone at the minimum zone range  $2X = 64.34$  km. Also the pulse is long enough to cover the whole zone. The angle 87.1 degrees corresponds with the minimum range point on curve  $d$  for the principal ray fan, Fig. 5. If symbols are introduced descriptive of the potential at  $r_m$ , the total potential  $\varphi_Z$  at the zone can be written

$$\begin{aligned} \varphi_Z &= \sum_1^N \left[ \frac{A}{r_n} e^{ik(ct-r_n)} \left( \frac{r_m}{r_n} e^{-ik(r_n-r_m)} \right) \right] \\ &= \frac{A}{r_m} e^{ik(ct-r_m)} \sum_1^N \frac{r_m}{r_n} e^{-ik(r_n-r_m)}. \end{aligned}$$

The ray, curved or not, is always assumed to be normal to its associated front at a point called here the trace point. It is the trace point which describes the ray. Between the source and the zone point  $x_n, z_o$ , the several cooperating trace points travel nearly the same horizontal distance  $2X$  but travel different ray distances  $r_n$  with different retarded phases, as if rays were coming from separate images. They are able to overlap and add potentials if they have sufficiently long wave trains. In comparing the contribution of the several ray fans to the zone potential in the present special case,  $r_m$ , by arbitrary choice, is always smaller than  $r_n$  so that  $r_m/r_n < 1$  and is nearly equal to unity because of the small angles (e.g., 0 to 7.8 degrees) involved in ray slopes. When the terms defined below are introduced, then

$$\varphi_Z = \varphi_m \sum_1^N (r_m/r_n) e^{-i2\pi b_n} = \varphi_m \Sigma_Z$$

where

$$\varphi_m = \frac{A}{r_m} e^{ik(ct-r_m)}$$

and

$$\frac{r_m}{r_n} < 1, \text{ but } \frac{r_m}{r_n} \approx 1.$$

Also,

$$\Delta r_n = (r_n - r_m)$$

so

$$\frac{\Delta r_n}{\lambda} = a + b_n$$

where  $a$  is an integer and  $0 < b_n < 1$ . The number  $N$  of waves cooperating at one zone point is small, with a maximum of eight, so that  $0 < N \leq 8$ . This is illustrated by the crossings in Fig. 5. The velocity potential  $\varphi_Z$  at a selected zone point where there are  $N$  crossings is illustrated by the minimum range potential  $\varphi_m$  multiplied by the complex sum

$$\Sigma_Z = \sum_1^N e^{-i2\pi b_n}.$$

The sum consists of eight or less unity-amplitude complex numbers with phases distributed in a specific way between zero and  $2\pi$ , at a particular instant, at the selected range point. If the numbers are arranged in sequence according to increasing phase, the complex multiplier  $\Sigma_Z$  may be represented by the sum of a spiral in the complex plane. This sum  $\Sigma_Z$  is an amplitude factor which multiplies the minimum range potential  $\varphi_m$  to give the potential at the selected zone point. The factor  $\Sigma_Z$  depends upon the geometry of the exeriment and refraction conditions existing in the ocean at the time of measurement. It is reasonable to assume that  $\Sigma_Z$  will change slowly with time in comparison with the time factor  $e^{ikct}$  in  $\varphi_m$ . The rapid signal oscillation,  $f = \omega/2\pi$ , is the frequency at which the source was driven. The amplitude factor  $\Sigma_Z$  causes the signal amplitude to wax and wane with the quasi frequency of fluctuation between zero, when the potentials add to zero, and  $N$  when all the wave potentials have the same phase. The number  $N$  of wave trains insonifying the zone governs the size of the maximum fluctuation amplitude, provided of course that the pulse length (773 m) is great enough for all the cooperating fans to overlap at the hydrophone not only in fan width but also in fan radial length. An overlap in both pulse time and pulse length is probable because of the fact that all rays considered are confined to the narrow convergence bundle.

The sound pressure is given by

$$p = \rho \dot{\varphi}$$

where the density of the sea water is  $\rho$ . The resultant pressure  $p_Z$  at the zone is given by the expression

$$p_Z = \rho \dot{\varphi}_Z = \rho [\dot{\varphi}_m \Sigma_Z + \varphi_m (\partial/\partial t) \Sigma_Z].$$

The sum  $\Sigma_Z$  is a slow function of the time as compared with the driving frequency so that  $(\partial/\partial t)\Sigma_Z$  may be considered to be zero. When the time derivative of  $\varphi_m$  is introduced, then

$$p_Z = ikc \rho \varphi_m \Sigma_Z = i\omega \varphi_m \Sigma_Z.$$

The pressure  $p_Z$  is proportional to the angular frequency  $\omega$ , the reference potential  $\varphi_m$ , and the sum  $\Sigma_Z$ . At a fluctuation maximum,  $\Sigma_Z$  is equal to  $N$ . The corresponding fluctuation maximum of pressure now designated by  $p_N$  is given by  $p_N = i\omega N \varphi_m$  and  $\varphi_m$  can be related to reference pressure  $p_o$  at  $r_o$ , which is usually the standard distance of 1 m, by the relation  $r_m \varphi_m = r_o \varphi_o$ . Then

$$\begin{aligned} p_N &= i\omega N r_o \varphi_o r_m^{-1} \\ &= r_o p_o r_m^{-1} N. \end{aligned}$$

The reference range  $r_m$  need not be taken at the convergence minimum;  $r_m$  could just as well represent a median value, thus reducing somewhat the error but complicating slightly the interpretation of  $\Sigma_Z$ .

The electrical potential  $v$  across the terminals of the hydrophone immersed in the sound field at the time of a fluctuation maximum is then given by the expression

$$v = k N p_o r_o r_m^{-1} \quad (5)$$

where

$v$  = electrical potential in volts at the hydrophone terminals,

$k$  = hydrophone calibration number in volts per dyne per  $\text{cm}^2$ ,

$N$  = an integer representing the number of wave fronts or rays or zone crossings at a point in the zone,

$p_o$  = source strength in dynes per  $\text{cm}^2$  at a distance of one meter from the radiation center ( $p_o = 2.24 \times 10^5$  dynes/ $\text{cm}^2$ ), and

$r_m$  = radial distance in meters from source to reference zone point  $r_m$ .

There was some doubt as to the existing value of the source strength  $p_o$ . Consequently, it was newly determined from short-range measurement of the acoustic field. The source was held at 70 ft depth (4). The hydrophone readings exhibited the normal interference variation. The shallow, well-developed first maximum at 120 ft depth, taken to represent  $p_N$ , gave a hydrophone reading of  $5.62 \times 10^{-2}$  volt, or 95 db;  $\mu\text{volt}$ .\* Two fronts, one direct, the other from the surface image, appeared to meet the hydrophone in phase at the depth of 120 feet. The slant range  $r$ , because of the shallow angle, is the same as the horizontal range to within 0.3 ft. This difference is neglected so that  $r = 1005$  m.

## FIELD MEASUREMENTS

Equation (5) may be rearranged to give the source strength  $p_o$  as

\*First maximum on Fig. 2, Ref. 4.

$$P_o = \frac{Vr_m}{kNr_o}$$

The formula developed for zone crossings will now be used for the simpler case of the close-in interference pattern developed by two rays. The measured quantities are

$$V = 5.62 \times 10^{-2} \text{ volt (53 db:dyne/cm}^2\text{)*}$$

$$r_m = 1005 \text{ meters}$$

$$k = 1.26 \times 10^{-4} \text{ volt/dyne per cm}^2$$

$$N = 2$$

$$r_o = 1 \text{ meter}$$

$$P_o = \frac{5.62 \times 10^{-2} \times 1.005 \times 10^3}{1.26 \times 10^{-4} \times 2}$$

$$= 2.24 \times 10^5 \text{ dynes per cm}^2 \text{ at one meter, or } 107 \text{ db:dynes/cm}^2 \text{ at one meter.}$$

Although the above source strength  $p_o$  determined from short-range measurements differs from the 95-db value of Ref. 4, it will now be used to determine  $N$ , the number of crossings at the zone.

A series of hydrophone voltages measured in the zone are given in Table 5. Equation (5) will be used to calculate the crossings. In this case  $r_m$  in the formula will be the zone point range listed as  $r$  in the table. The quantity  $(kp_o r_o)^{-1}$  is the same for each range and equals  $3.55 \times 10^{-2}$ . Consequently,  $N = 3.55 \times 10^{-2} V r_m$ .

All values of  $N$  in Table 5 are small numbers which fall within the range of integers from 1 to 8, exhibited by the stepped line of Fig. 5. The tabulated values of  $N$  are added to Fig. 5 as circles which fall nearly enough to the stepped line to encourage the conviction that the principles on which crossings were estimated are sound.

Table 5  
Calculated vs Measured Zone Crossings

Zone Range $r$ (km)	Hydrophone Readings $v$ of the Acoustic Signal (mv)	Number of Zone Crossings $N$	
		Measured	Calculated
62.8	0.63	1.41	-
63.6	0.56	1.27	-
64.5	1.57	3.60	2
65.5	1.41	3.28	2
66.3	1.78	4.19	4
67.7	1.12	2.69	5
68.0	3.01	7.27	7
69.5	0.89	2.20	6
70.5	1.78	4.45	6

\*First maximum on Fig. 2, Ref. 4.

The first two points indicate the possible existence of radiation of about one ray prior to the onset of the 64.34 minimum range at which the points indicate a jump of about the right amount of two units, which is maintained until near 66 km. The next point at 66.3 km has the correct value of about four for that step. Unfortunately, the range increments were not fine enough to reveal the interesting detail of the jump to eight units.

Between  $2X = 66.3$  km and  $2X = 67.7$  km there is a long gap in observations so that the interesting high values in the stepped line (of as much as eight crossings) lack observational confirmation. The low circle at 67.7 km does, however, tend to confirm the sharp predicted drop between 67.6 km and 67.8 km. Also, the 7.3 circle at 68 km checks well with the step of seven units. Circles 2.2 at 69.5 km and 4.5 at 70.5 km seem to foreshadow the final drop in the stepped line to near unity. Force speculation as to the explanation of agreement and divergencies is idle, especially in view of the fact that the way is now indicated whereby other and more detailed field observations can be made. It is interesting to note, however, that the maximum enhancement of pressure in the zone is a factor of eight over free-field inverse-distance spreading of pressure. This is a "gain" of 18 db.

#### ACKNOWLEDGMENTS

Confirmation of predictions is based upon the field data gathered by Clark W. Searfoss, Section Head for Ocean Sound Propagation at the U.S. Naval Research Laboratory. Considerable assistance was rendered by David L. Jacobson and B. J. Holloway in computations and curve plotting. Alan H. Rich assembled the computer program for computation of sound speed from the function  $c(T, D, S)$ .

The experimental data in this report and in NRL Report 6123 were gathered with the assistance of the USS GROUPE (AGSS214) and the USS ROCKVILLE (EPCER 851).

#### REFERENCES

1. Steinberger, R.L., "Computation of Acoustic Rays from Temperatures Measured in the Deep Ocean and Prediction of the Range to the Convergence Zone," NRL Report 6123, Aug. 1964
2. Bryant, R.W., and Sorensen, N.R., "Application of a Bilinear Velocity Profile to Convergence Zone Transmission," NRL Report 4834, Oct. 1956
3. "Handbook of Mathematical Tables," 1st ed., supplement to "Handbook of Chemistry and Physics," Cleveland:Chemical Rubber Publishing Co., 1962
4. Searfoss, C.W., "Fluctuation of 1/2-Second Pulses of Low Frequency Sound in the Open Ocean," NRL Report 5718 (Confidential Report, Unclassified Title), Dec. 1961

## DOCUMENT CONTROL DATA - R&amp;D

(Security classification of title, body of abstract and indexing annotation must be entered when the overall report is classified)

1. ORIGINATING ACTIVITY (Corporate author)		2a. REPORT SECURITY CLASSIFICATION	
U.S. Naval Research Laboratory Washington, D.C. 20390		Unclassified	
		2b. GROUP	
3. REPORT TITLE			
COMPARISON OF CONVERGENCE-ZONE-MEASURED SOUND PRESSURES IN THE DEEP OCEAN WITH PRESSURES COMPUTED FROM THE SOUND SPEED-DEPTH FUNCTION			
4. DESCRIPTIVE NOTES (Type of report and inclusive dates)			
An interim report on one phase of the problem.			
5. AUTHOR(S) (Last name, first name, initial)			
Steinberger, R.L.			
6. REPORT DATE		7a. TOTAL NO. OF PAGES	7b. NO. OF REFS
August 5, 1965		28	4
8a. CONTRACT OR GRANT NO.		9a. ORIGINATOR'S REPORT NUMBER(S)	
NRL Problem S01-01		NRL Report 6269	
b. PROJECT NO.		9b. OTHER REPORT NO(S) (Any other numbers that may be assigned this report)	
RF 101-03-45-5250			
c.			
d.			
10. AVAILABILITY/LIMITATION NOTICES			
Unlimited Availability - Available from CFSTI			
11. SUPPLEMENTARY NOTES		12. SPONSORING MILITARY ACTIVITY	
		Department of the Navy (Office of Naval Research)	
13. ABSTRACT			
<p>This report is a sequel to an earlier report (NRL Report 6123) in which the sound speed <math>c</math> was determined as a function of the depth <math>z</math> in deep-ocean waters north of Puerto Rico. Computational methods were also developed and used to obtain numerical values for the horizontal range between the sound source and the zone where the emitted acoustic waves converge to give signal (pressure) enhancement. The present report is concerned with computing the detailed distribution of sound pressure, by means of ray diagrams and field measurements, in the zone. On the basis of simple wave theory, convergence zone ranges and pressure values are derived from the <math>c(z)</math> function for three basic ray fans which overlap at the zone. It is found that both the horizontal range determinations (from 64.34 to about 70 km) and the acoustic pressure values within the zone agree favorably with measured values. By utilizing deep-ocean measurements, the resultant acoustic pressures were free of confusion from bottom scattering and the complexity of many refraction paths.</p>			

14. KEY WORDS	LINK A		LINK B		LINK C	
	ROLE	WT	ROLE	WT	ROLE	WT
Underwater sound Sound transmission Refraction Reflection Pressure-Measurement Wave transmission-Theory Acoustics						

**INSTRUCTIONS**

**1. ORIGINATING ACTIVITY:** Enter the name and address of the contractor, subcontractor, grantee, Department of Defense activity or other organization (*corporate author*) issuing the report.

**2a. REPORT SECURITY CLASSIFICATION:** Enter the overall security classification of the report. Indicate whether "Restricted Data" is included. Marking is to be in accordance with appropriate security regulations.

**2b. GROUP:** Automatic downgrading is specified in DoD Directive 5200.10 and Armed Forces Industrial Manual. Enter the group number. Also, when applicable, show that optional markings have been used for Group 3 and Group 4 as authorized.

**3. REPORT TITLE:** Enter the complete report title in all capital letters. Titles in all cases should be unclassified. If a meaningful title cannot be selected without classification, show title classification in all capitals in parenthesis immediately following the title.

**4. DESCRIPTIVE NOTES:** If appropriate, enter the type of report, e.g., interim, progress, summary, annual, or final. Give the inclusive dates when a specific reporting period is covered.

**5. AUTHOR(S):** Enter the name(s) of author(s) as shown on or in the report. Enter last name, first name, middle initial. If military, show rank and branch of service. The name of the principal author is an absolute minimum requirement.

**6. REPORT DATE:** Enter the date of the report as day, month, year, or month, year. If more than one date appears on the report, use date of publication.

**7a. TOTAL NUMBER OF PAGES:** The total page count should follow normal pagination procedures, i.e., enter the number of pages containing information.

**7b. NUMBER OF REFERENCES:** Enter the total number of references cited in the report.

**8a. CONTRACT OR GRANT NUMBER:** If appropriate, enter the applicable number of the contract or grant under which the report was written.

**8b, 8c, & 8d. PROJECT NUMBER:** Enter the appropriate military department identification, such as project number, subproject number, system numbers, task number, etc.

**9a. ORIGINATOR'S REPORT NUMBER(S):** Enter the official report number by which the document will be identified and controlled by the originating activity. This number must be unique to this report.

**9b. OTHER REPORT NUMBER(S):** If the report has been assigned any other report numbers (*either by the originator or by the sponsor*), also enter this number(s).

**10. AVAILABILITY/LIMITATION NOTICES:** Enter any limitations on further dissemination of the report, other than those

imposed by security classification, using standard statements such as:

- (1) "Qualified requesters may obtain copies of this report from DDC."
- (2) "Foreign announcement and dissemination of this report by DDC is not authorized."
- (3) "U. S. Government agencies may obtain copies of this report directly from DDC. Other qualified DDC users shall request through \_\_\_\_\_."
- (4) "U. S. military agencies may obtain copies of this report directly from DDC. Other qualified users shall request through \_\_\_\_\_."
- (5) "All distribution of this report is controlled. Qualified DDC users shall request through \_\_\_\_\_."

If the report has been furnished to the Office of Technical Services, Department of Commerce, for sale to the public, indicate this fact and enter the price, if known.

- 11. SUPPLEMENTARY NOTES:** Use for additional explanatory notes.
- 12. SPONSORING MILITARY ACTIVITY:** Enter the name of the departmental project office or laboratory sponsoring (*paying for*) the research and development. Include address.
- 13. ABSTRACT:** Enter an abstract giving a brief and factual summary of the document indicative of the report, even though it may also appear elsewhere in the body of the technical report. If additional space is required, a continuation sheet shall be attached.

It is highly desirable that the abstract of classified reports be unclassified. Each paragraph of the abstract shall end with an indication of the military security classification of the information in the paragraph, represented as (*TS*), (*S*), (*C*), or (*U*).

There is no limitation on the length of the abstract. However, the suggested length is from 150 to 225 words.

**14. KEY WORDS:** Key words are technically meaningful terms or short phrases that characterize a report and may be used as index entries for cataloging the report. Key words must be selected so that no security classification is required. Identifiers, such as equipment model designation, trade name, military project code name, geographic location, may be used as key words but will be followed by an indication of technical context. The assignment of links, rules, and weights is optional.